Supplementary information

Quantum spin nematic phase in a square-lattice iridate

Supplementary Information:

Quantum spin nematic phase in a square-lattice iridate

Hoon Kim,[1,2,*] Jin-Kwang Kim,[1,2,*] Junyoung Kwon,[2] Jimin Kim,[1,2]

Hyun-Woo J. Kim,[1,2] Seunghyeok Ha,[1,2] Kwangrae Kim,[1,2] Wonjun Lee,[1,2]

Jonghwan Kim,[3,4] Gil Young Cho,[1,2] Hyeokjun Heo,[5] Joonho Jang,[5]

Ch. J. Sahle,[6] A. Longo,[6,7] J. Strempfer,[8] G. Fabbris,[8] Y. Choi,[8] D. Haskel,[8]

Jungho Kim,[8] J. W. Kim,[8] B. J. Kim,[1,2,†]

[1]Center for Artificial Low Dimensional Electronic Systems,

Institute for Basic Science (IBS), 77 Cheongam-Ro, Pohang 37673, South Korea

[2]Department of Physics, Pohang University of Science and Technology,

Pohang 37673, South Korea

[3]Center for Van der Waals Quantum Solids,

Institute for Basic Science (IBS), Pohang, 37673, Korea

[4]Department of Materials Science and Engineering,

Pohang University of Science and Technology, Pohang 37673, Korea

[5]Department of Physics and Astronomy,

Seoul National University, Seoul 08826, South Korea

[6]ESRF, The European Synchrotron, 71 Avenue des

Martyrs, CS40220, 38043 Grenoble Cedex 9, France

[7]Istituto per lo Studio dei Materiali Nanostrutturati,

Consiglio Nazionale Delle Ricerche, Palermo, I-90146, Italy

[8]Advanced Photon Source, Argonne National Laboratory, Argonne, Illinois 60439, USA

[*]These authors contributed equally to this work.

[†]To whom correspondence should be addressed; E-mail: bjkim6@postech.ac.kr

INDEX

1. Circular dichroism in RXD

We show here that within $E1$-$E1$ transition CD can only arise when electric quadrupole and magnetic dipole are both present.

The scattering intensity of RXD is given by

$$I \propto |\Sigma_j \exp(i\mathbf{Q} \cdot \mathbf{r}_j) f^j_{\alpha\beta} \epsilon'^*_\alpha \epsilon_\beta|^2 = |F_{\alpha\beta} \epsilon'^*_\alpha \epsilon_\beta|^2 \,, \tag{S1}$$

where f is the atomic form factor given by a 3×3 matrix, $F_{\alpha\beta} = \Sigma_j \exp(i\mathbf{Q} \cdot \mathbf{r}_j) f^j_{\alpha\beta}$, ϵ (ϵ') denotes the incoming (outgoing) light polarization vector and $\alpha(\beta) \in \{x, y, z\}$. Noting that both F and ϵ are complex, we write

$$F_{\alpha\beta} = F_{1,\alpha\beta} + iF_{2,\alpha\beta} \,, \tag{S2}$$

$$e_{\alpha\beta} = e_{1,\alpha\beta} + ie_{2,\alpha\beta} \,, \tag{S3}$$

where $e_{\alpha\beta} \equiv \epsilon'^*_\alpha \epsilon_\beta$. We omit the α and β indices below for clarity. Then the scattering intensity becomes

$$\begin{aligned} I \propto |F_{\alpha\beta} e_{\alpha\beta}|^2 &= |(F_1 + iF_2)(e_1 + ie_2)|^2 \\ &= |F_1 e_1 - F_2 e_2|^2 + |F_2 e_1 + F_1 e_2|^2 \\ &= (F_1 e_1)^2 + (F_2 e_2)^2 - 2(F_1 e_1)(F_2 e_2) + (F_2 e_1)^2 + (F_1 e_2)^2 + 2(F_2 e_1)(F_1 e_2) \,. \end{aligned} \tag{S4}$$

For circularly polarized light, $e_1 \to e_1$ and $e_2 \to -e_2$ under $LL \to RR$ or $LR \to RL$. Therefore,

$$I_{DIFF} \propto (F_1 e_1)(F_2 e_2) - (F_2 e_1)(F_1 e_2). \tag{S5}$$

Next, noting that time-reversal even quadrupole (time-reversal odd magnetic dipole) is represented by symmetric (antisymmetric) components of the atomic form factor tensor, we define

$$F_{1,2} = F^S_{1,2} + F^A_{1,2} \,, \tag{S6}$$

$$e_{1,2} = e^S_{1,2} + e^A_{1,2} \,, \tag{S7}$$

where S (A) denotes the symmetric (antisymmetric) component of the tensor. Then we arrive at

$$\begin{aligned} I_{DIFF} \propto\ & (F^S_1 e^S_1 + F^A_1 e^A_1)(F^S_2 e^S_2 + F^A_2 E^A_2) - (F^S_2 e^S_1 + F^A_2 e^A_1)(F^S_1 e^S_2 + F^A_1 e^A_2) \\ =\ & F^S_1 e^S_1 F^S_2 e^S_2 + F^A_1 e^A_1 F^S_2 e^S_2 + F^S_1 e^S_1 F^A_2 e^A_2 + F^A_1 e^A_1 F^A_2 e^A_2 \\ &- (F^S_2 e^S_1 F^S_1 e^S_2 + F^A_2 e^A_1 F^S_1 e^S_2 + F^S_2 e^S_1 F^A_1 e^A_2 + F^A_2 e^A_1 F^A_1 e^A_2) \,. \end{aligned} \tag{S8}$$

Further simplication is possible when $F_1^S = \pm F_2^S$ and $F_1^A = \pm F_2^A$, in which case $F_1^S(F_1^A)$ and $F_2^S(F_2^A)$ can be interchanged. This is the case for $\mathbf{Q} = (0\,0\,odd)$ reflections as explicitly confirmed in Table S4 for all possible quadrupole structures with non-zero structure factors. Then, the CD intensity becomes

$$I_{DIFF} \propto F_1^M e_1^A F_2^Q e_2^S + F_1^Q e_1^S F_2^M e_2^A - F_2^M e_1^A F_1^Q e_2^S - F_2^Q e_1^S F_1^M e_2^A \ , \tag{S9}$$

where we identify $F_{1,2}^Q = F_{1,2}^S$ and $F_{1,2}^M = F_{1,2}^A$. Thus, the CD in our case, under the assumption that only $E_1 - E_1$ process is relevant, can only arise from the interference between magnetic and quadrupolar orders.

2. Other mechanisms of circular dichroism

Here, we discuss other known origins of CD in RXD and show that they are irrelevant to our case. In Fig. S1, we first compare the CD response of ferromagnetic $(0\,0\,odd)$ reflections to that of antiferromagnetic $(1\,0\,4n+2)$ reflections. The reflections $(0\,0\,21)$ and $(1\,0\,18)$ are chosen as to have similar scattering geometries, and the CD differences $I_{RC} - I_{LC}$ are normalized by the magnetic diffraction peak intensity. Unlike $(0\,0\,21)$ reflection exhibiting a clear CD at the resonance, we find no indication of CD on $(1\,0\,18)$ reflection. This rules out extrinsic sources of CD, such as birefringence [1].

As for intrinsic mechanisms, there are three physically distinct origins for CD: (i) a chiral lattice structure [2–4] or a helical magnetic structure [5–7], where CD arises from a single type of scattering entity; (ii) interference between two distinct types of scatterers within E1-E1 process; (iii) higher-order processes such as electric dipole-magnetic dipole (E1-M1). The E1-M1 contribution, however, is smaller by a factor of $10^{-3} \sim 10^{-4}$ compared to the leading E1-E1 contribution [8], and thus cannot produce CD of the order of $1\,\%$ as observed. Further, case (i) is clearly irrelevant to Sr_2IrO_4 [9], as lattice is centrosymmetric and the magnetic structure also preserves the inversion symmetry of the lattice. Therefore, CD can only be explained by dipole-quadrupole interference within the E1-E1 process. We also note that the Templeton-Templeton scattering, also known as anisotropy-of-tensor of susceptibility (ATS) scattering [10], is irrelevant since it is not allowed for the body-center-translation odd
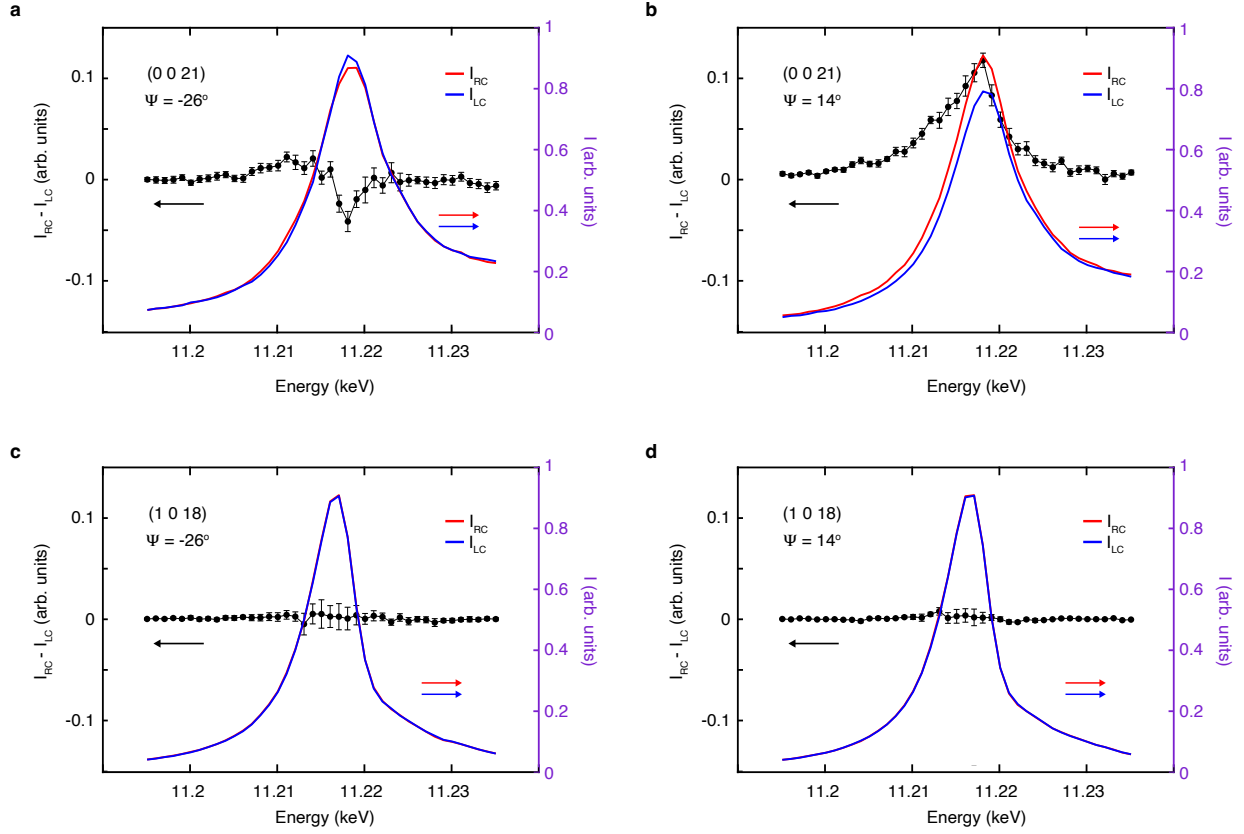
FIG. S1. **CD-RXD on magnetic reflections. a, b,** (0 0 odd) magnetic reflections exhibit a clear CD through interference between dipolar and quadrupolar moments, **c, d,** whereas the CD signals are not manifested for (1 0 $4n+2$) reflections of similar scattering geometry.

reflection $\mathbf{q} = (0\,0\,21)$.

3. Representation analysis for bond-centered quadrupolar orders

We systematically look for all symmetry-allowed $\mathbf{q}=0$ bond-centered quadrupolar orders. The crystal structure of Sr_2IrO_4 has $I4_1/acd$ space group (No. 142) consisting of 32 symmetry elements and their direct product with the translation group [11, 12]. For the Γ-point of the conventional unit cell, the factor group G/T, where T is the translation subgroup excluding the body-center translation of the space group G, has eight one-dimensional (1D) and six 2D irreducible representations (IRs). The character table is shown in Table S1.

Class	g	A_{1g}	A_{1u}	A_{2g}	A_{2u}	B_{1g}	B_{1u}	B_{2g}	B_{2u}	E_g	E_u	Γ_1	Γ_2	Γ_3	Γ_4
							Irreducible Representations								
$\{E\|0\}$	1	1	1	1	1	1	1	1	1	2	2	2	2	2	2
$\{C_2\|(0,0,\frac{1}{2})\}$	2	1	1	1	1	1	1	1	1	-2	-2	2	2	-2	-2
$4\{C_4\|(0,0,\frac{1}{4})\}$	3,4,19,20	1	1	1	1	-1	-1	-1	-1	0	0	0	0	0	0
$2\{C_{2\perp}\|0\}$	5,6	1	1	-1	-1	1	1	-1	-1	0	0	-2	-2	0	0
$4\{C_{2'}\|(\frac{1}{2},\frac{1}{2},0)\}$	7,8,23,24	1	1	-1	-1	-1	-1	1	1	0	0	0	0	0	0
$2\{I\|0\}$	9,25	1	-1	1	-1	1	-1	1	-1	2	-2	0	0	0	0
$2\{\sigma_h\|(\frac{1}{2},0,0)\}$	10,26	1	-1	1	-1	1	-1	1	-1	-2	2	0	0	0	0
$4\{S_4\|0\}$	11,12,27,28	1	-1	1	-1	-1	1	-1	1	0	0	0	0	0	0
$2\{\sigma_v\|(\frac{1}{2},0,0)\}$	13,30	1	-1	-1	1	1	-1	-1	1	0	0	0	0	-2	2
$2\{\sigma_v\|(0,0,\frac{1}{2})\}$	14,29	1	-1	-1	1	1	-1	-1	1	0	0	0	0	2	-2
$4\{\sigma_d\|(\frac{1}{4},\frac{1}{4},\frac{1}{4})\}$	15,16,31,32	1	-1	-1	1	-1	1	1	-1	0	0	0	0	0	0
$\{E\|(\frac{1}{2},\frac{1}{2},\frac{1}{2})\}$	17	1	1	1	1	1	1	1	1	2	2	-2	-2	-2	-2
$\{C_2\|0\}$	18	1	1	1	1	1	1	1	1	-2	-2	-2	-2	2	2
$2\{C_{2\perp}\|(\frac{1}{2},0,0)\}$	21,22	1	1	-1	-1	1	1	-1	-1	0	0	-2	2	0	0

TABLE S1. **Character table of $I4_1/acd$ space group (No. 142).** The rows and columns correspond to the classes and the irreducible representations, respectively. The second column lists for each class the symmetry elements, which are numbered as in the international tables for crystallography [11].

All of the IRs that are invariant against the body-center translation $\{E|(\frac{1}{2},\frac{1}{2},\frac{1}{2})\}$ are

labeled in terms of the IRs of the point group of the space group, whereas the remaining four 2D IRs that change their sign upon the body-center translation are labeled as Γ_1 through Γ_4. These provide a complete basis set for all possible symmetry breaking orders that do not enlarge the unit cell. For example, an arbitrary magnetic order can be expressed by eight axial vectors placed at each position of the eight Ir ions in the unit cell; i.e., a real vector in the $3 \times 8 = 24$ dimensional space, which can be reduced to $A_{1g} \oplus A_{2g} \oplus B_{1u} \oplus B_{2u} \oplus 2E_g \oplus 2E_u \oplus 2\Gamma_1 \oplus 2\Gamma_2 \oplus \Gamma_3 \oplus \Gamma_4$ (for detailed representation analysis of the magnetic order, see Supplementary information in [13]). Among them, the Γ_1 magnetic structure is experimentally confirmed by RXD [14] and neutron diffraction [9] (see Fig. S2b).

Similarly, an arbitrary bond-centered quadrupolar order can be expressed by sixteen rank-two cubic tensors placed at the sixteen nearest-neighbour (NN) bond-centers in the unit cell
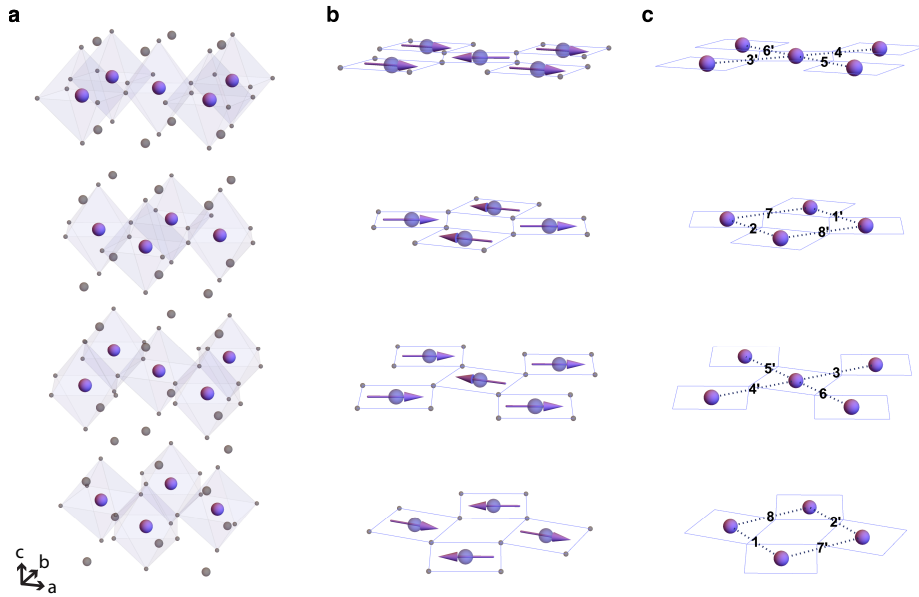

FIG. S2. **Crystal and magnetic structures of Sr_2IrO_4. a, b,** The crystal (**a**) and magnetic (**b**) structure of Sr_2IrO_4. Iridium ions and moments are colored by purple. **c,** Bond centers between nearest neighbors are numbered. Primed numbers indicate bond centers connected by the body-center translation.

(at $16f$ Wyckoff-positions), each of which carries five quadrupolar degrees of freedom

$$
\begin{pmatrix}
S_i^x S_j^x - S_i^y S_j^y \\
\frac{1}{\sqrt{3}}(2S_i^z S_j^z - S_i^x S_j^x - S_i^y S_j^y) \\
S_i^x S_j^y + S_i^y S_j^x \\
S_i^y S_j^z + S_i^z S_j^y \\
S_i^z S_j^x + S_i^x S_j^z
\end{pmatrix} ,
\tag{S10}
$$

where i and j are the NN iridium ions. They lead to a representation of 80 by 80 matrices, which can be reduced into the following IRs:

$$
3A_{1g} \oplus 3A_{1u} \oplus 2A_{2g} \oplus 2A_{2u} \oplus 2B_{1g} \oplus 2B_{1u} \oplus 3B_{2g} \oplus 3B_{2u}
$$

$$
\oplus 5E_g \oplus 5E_u \oplus 5\Gamma_1 \oplus 5\Gamma_2 \oplus 5\Gamma_3 \oplus 5\Gamma_4 .
\tag{S11}
$$

For quadrupolar orders with E_g and Γ_1 symmetry, Table S2 shows the basis vectors, whose transformation matrices are listed in Table S3.

Based on the Raman results, provided that only Q_{yz} $(S_i^y S_j^z + S_i^z S_j^y)$ and Q_{zx} $(S_i^z S_j^x + S_i^x S_j^z)$ can couple to the light polarizations ϵ_{yz} and ϵ_{zx}, respectively, there are only two possible quadrupolar structures, which have either ferroquadrupolar ($q_4 \neq 0$) or antiferroquadrupolar ($q_5 \neq 0$; see Fig. S3) pattern within the layers.
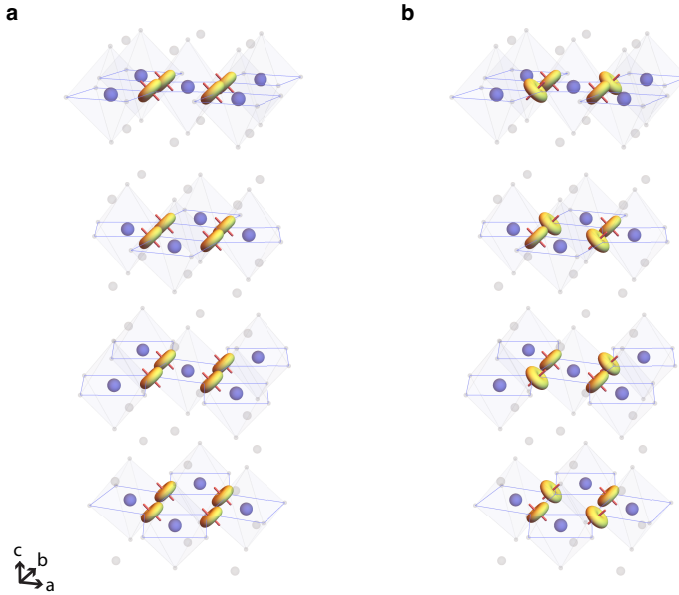

FIG. S3. **Ferroquadrupolar and antiferroquadrupolar orders. a, b,** E_g symmetry quadrupolar orders with ferroquadrupolar (**a**) and antiferroquadrupolar (**b**) configuration of Q_{zx} moments.

BCs	E_g		Γ_1	
	E_{gu}	E_{gv}	Γ_{1u}	Γ_{1v}
1	$(q_1,\ q_2,\ q_3,\ q_4,\ q_5)$	$(q_1,\ -q_2,\ -q_3,\ q_5,\ q_4)$	$(q_1,\ q_2,\ q_3,\ q_4,\ q_5)$	$(q_1,\ -q_2,\ -q_3,\ q_5,\ q_4)$
2	$(-q_1,\ -q_2,\ -q_3,\ q_4,\ q_5)$	$(-q_1,\ q_2,\ q_3,\ q_5,\ q_4)$	$(q_1,\ q_2,\ q_3,\ -q_4,\ -q_5)$	$(q_1,\ -q_2,\ -q_3,\ -q_5,\ -q_4)$
3	$(-q_1,\ -q_2,\ q_3,\ q_4,\ -q_5)$	$(q_1,\ -q_2,\ q_3,\ -q_5,\ q_4)$	$(-q_1,\ -q_2,\ q_3,\ q_4,\ -q_5)$	$(-q_1,\ q_2,\ -q_3,\ q_5,\ -q_4)$
4	$(q_1,\ q_2,\ -q_3,\ q_4,\ -q_5)$	$(-q_1,\ q_2,\ -q_3,\ -q_5,\ q_4)$	$(-q_1,\ -q_2,\ q_3,\ -q_4,\ q_5)$	$(-q_1,\ q_2,\ -q_3,\ -q_5,\ q_4)$
5	$(q_1,\ q_2,\ q_3,\ q_4,\ q_5)$	$(q_1,\ -q_2,\ -q_3,\ q_5,\ q_4)$	$(-q_1,\ -q_2,\ -q_3,\ -q_4,\ -q_5)$	$(q_1,\ -q_2,\ -q_3,\ q_5,\ q_4)$
6	$(-q_1,\ -q_2,\ -q_3,\ q_4,\ q_5)$	$(-q_1,\ q_2,\ q_3,\ q_5,\ q_4)$	$(-q_1,\ -q_2,\ -q_3,\ q_4,\ q_5)$	$(q_1,\ -q_2,\ -q_3,\ -q_5,\ -q_4)$
7	$(-q_1,\ -q_2,\ q_3,\ q_4,\ -q_5)$	$(q_1,\ -q_2,\ q_3,\ -q_5,\ q_4)$	$(q_1,\ q_2,\ -q_3,\ -q_4,\ q_5)$	$(-q_1,\ q_2,\ -q_3,\ q_5,\ -q_4)$
8	$(q_1,\ q_2,\ -q_3,\ q_4,\ -q_5)$	$(-q_1,\ q_2,\ -q_3,\ -q_5,\ q_4)$	$(q_1,\ q_2,\ -q_3,\ q_4,\ -q_5)$	$(-q_1,\ q_2,\ -q_3,\ -q_5,\ q_4)$

TABLE S2. **The basis vectors of E_g and Γ_1 bond-center quadrupolar orders.** Bond centers (BCs) are indicated in Fig. S2c. q_i (i=1,$\cdots$,5) are independent parameters for quadrupolar moments.

Matrix representation	$\begin{pmatrix} 1 & 0 \\ 0 & 1 \end{pmatrix}$	$\begin{pmatrix} 0 & 1 \\ 1 & 0 \end{pmatrix}$	$\begin{pmatrix} -1 & 0 \\ 0 & 1 \end{pmatrix}$	$\begin{pmatrix} 0 & -1 \\ 1 & 0 \end{pmatrix}$
Symmetry elements for E_g	$1, 9, 17, 25$	$8, 16, 24, 32$	$5, 13, 21, 29$	$4, 12, 20, 28$
Symmetry elements for Γ_1	$1, 2, 5, 6$	$3, 4, 7, 8$	$9, 10, 13, 14$	$11, 12, 15, 16$

Matrix representation	$\begin{pmatrix} -1 & 0 \\ 0 & -1 \end{pmatrix}$	$\begin{pmatrix} 0 & -1 \\ -1 & 0 \end{pmatrix}$	$\begin{pmatrix} 1 & 0 \\ 0 & -1 \end{pmatrix}$	$\begin{pmatrix} 0 & 1 \\ -1 & 0 \end{pmatrix}$
Symmetry elements for E_g	$2, 10, 18, 26$	$7, 15, 23, 31$	$6, 14, 22, 30$	$3, 11, 19, 27$
Symmetry elements for Γ_1	$17, 18, 21, 22$	$19, 20, 23, 24$	$25, 26, 29, 30$	$27, 28, 31, 32$

TABLE S3. **Matrix representation of the symmetry elements for E_g and Γ_1 IRs.** The matrices are expressed in the $(u,\ v)$ basis in Table S2. The symmetry elements of $I4_1/acd$ space group are numbered as in the international tables for crystallography [11].

Next, we solve for possible quadrupole structures consistent with the CD-RXD results (Fig. 2). The reflection at $(0\,0\,21)$ implies that the order is odd under the body-center

translation symmetry, which in turn implies that the structure must be one of the four IRs: Γ_1, Γ_2, Γ_3 or Γ_4. We obtain five quadrupolar orders with non-vanishing scattering amplitude $(\Gamma_1 \oplus \Gamma_2 \oplus \Gamma_3 \oplus 2\Gamma_4)$, which are documented in Table S4. Using the scattering amplitudes F^Q (Table S4) and the magnetic structure in Fig. S2b, we simulate the azimuth-angle dependence of the CD signals at $(0\,0\,21)$ for different values of $s = rQ_{zx}/M_y$.

BC	$e^{i\mathbf{Q}\cdot\mathbf{r}}$	Γ_{1u} (Q_{yz})	Γ_{1v} (Q_{zx})
1	1	$(0, 0, 0, q_1, 0)$	$(0, 0, 0, 0, q_1)$
2	-1	$(0, 0, 0, -q_1, 0)$	$(0, 0, 0, 0, -q_1)$
3	i	$(0, 0, 0, q_1, 0)$	$(0, 0, 0, 0, -q_1)$
4	-i	$(0, 0, 0, -q_1, 0)$	$(0, 0, 0, 0, q_1)$
5	-i	$(0, 0, 0, -q_1, 0)$	$(0, 0, 0, 0, q_1)$
6	i	$(0, 0, 0, q_1, 0)$	$(0, 0, 0, 0, -q_1)$
7	-1	$(0, 0, 0, -q_1, 0)$	$(0, 0, 0, 0, -q_1)$
8	1	$(0, 0, 0, q_1, 0)$	$(0, 0, 0, 0, q_1)$

$$F^Q = \begin{pmatrix} 0 & 0 & 0 \\ 0 & 0 & c^*q_1 \\ 0 & c^*q_1 & 0 \end{pmatrix}$$

$$F^Q = \begin{pmatrix} 0 & 0 & cq_1 \\ 0 & 0 & 0 \\ cq_1 & 0 & 0 \end{pmatrix}$$

BC	$e^{i\mathbf{Q}\cdot\mathbf{r}}$	Γ_{2u} (Q_{zx})	Γ_{2v} (Q_{yz})
1	1	$(0, 0, 0, 0, q_1)$	$(0, 0, 0, -q_1, 0)$
2	-1	$(0, 0, 0, 0, -q_1)$	$(0, 0, 0, q_1, 0)$
3	i	$(0, 0, 0, 0, q_1)$	$(0, 0, 0, q_1, 0)$
4	-i	$(0, 0, 0, 0, -q_1)$	$(0, 0, 0, -q_1, 0)$
5	-i	$(0, 0, 0, 0, -q_1)$	$(0, 0, 0, -q_1, 0)$
6	i	$(0, 0, 0, 0, q_1)$	$(0, 0, 0, q_1, 0)$
7	-1	$(0, 0, 0, 0, -q_1)$	$(0, 0, 0, q_1, 0)$
8	1	$(0, 0, 0, 0, q_1)$	$(0, 0, 0, -q_1, 0)$

$$F^Q = \begin{pmatrix} 0 & 0 & c^*q_1 \\ 0 & 0 & 0 \\ c^*q_1 & 0 & 0 \end{pmatrix}$$

$$F^Q = \begin{pmatrix} 0 & 0 & 0 \\ 0 & 0 & -cq_1 \\ 0 & -cq_1 & 0 \end{pmatrix}$$

BC	$e^{i\mathbf{Q}\cdot\mathbf{r}}$	Γ_{3u} (Q_{xy})		Γ_{3v} (Q_{xy})	
1	1	$(0, 0, q_1, 0, 0)$		$(0, 0, q_1, 0, 0)$	
2	-1	$(0, 0, \text{-}q_1, 0, 0)$		$(0, 0, \text{-}q_1, 0, 0)$	
3	i	$(0, 0, \text{-}q_1, 0, 0)$		$(0, 0, q_1, 0, 0)$	
4	-i	$(0, 0, q_1, 0, 0)$		$(0, 0, \text{-}q_1, 0, 0)$	
5	-i	$(0, 0, q_1, 0, 0)$		$(0, 0, \text{-}q_1, 0, 0)$	
6	i	$(0, 0, \text{-}q_1, 0, 0)$		$(0, 0, q_1, 0, 0)$	
7	-1	$(0, 0, \text{-}q_1, 0, 0)$		$(0, 0, \text{-}q_1, 0, 0)$	
8	1	$(0, 0, q_1, 0, 0)$		$(0, 0, q_1, 0, 0)$	

$$F^Q = \begin{pmatrix} 0 & cq_1 & 0 \\ cq_1 & 0 & 0 \\ 0 & 0 & 0 \end{pmatrix}$$

$$\begin{pmatrix} 0 & c^*q_1 & 0 \\ c^*q_1 & 0 & 0 \\ 0 & 0 & 0 \end{pmatrix}$$

BC	$e^{i\mathbf{Q}\cdot\mathbf{r}}$	Γ_{4u} $(Q_{x^2-y^2}$ & $Q_{3z^2-r^2})$		Γ_{4v} $(Q_{x^2-y^2}$ & $Q_{3z^2-r^2})$	
1	1	$(q_1, q_2, 0, 0, 0)$		$(q_1, \text{-}q_2, 0, 0, 0)$	
2	-1	$(\text{-}q_1, \text{-}q_2, 0, 0, 0)$		$(\text{-}q_1, q_2, 0, 0, 0)$	
3	i	$(q_1, q_2, 0, 0, 0)$		$(\text{-}q_1, q_2, 0, 0, 0)$	
4	-i	$(\text{-}q_1, \text{-}q_2, 0, 0, 0)$		$(q_1, \text{-}q_2, 0, 0, 0)$	
5	-i	$(\text{-}q_1, \text{-}q_2, 0, 0, 0)$		$(q_1, \text{-}q_2, 0, 0, 0)$	
6	i	$(q_1, q_2, 0, 0, 0)$		$(\text{-}q_1, q_2, 0, 0, 0)$	
7	-1	$(\text{-}q_1, \text{-}q_2, 0, 0, 0)$		$(\text{-}q_1, q_2, 0, 0, 0)$	
8	1	$(q_1, q_2, 0, 0, 0)$		$(q_1, \text{-}q_2, 0, 0, 0)$	

$$c^* \cdot \begin{pmatrix} q_1 - \frac{q_2}{\sqrt{3}} & 0 & 0 \\ 0 & \text{-}q_1 - \frac{q_2}{\sqrt{3}} & 0 \\ 0 & 0 & \frac{2q_2}{\sqrt{3}} \end{pmatrix}$$

$$c \cdot \begin{pmatrix} q_1 + \frac{q_2}{\sqrt{3}} & 0 & 0 \\ 0 & \text{-}q_1 + \frac{q_2}{\sqrt{3}} & 0 \\ 0 & 0 & -\frac{2q_2}{\sqrt{3}} \end{pmatrix}$$

TABLE S4: **Bond-centered quadrupolar orders with non-zero scattering amplitudes F^Q at $(0\,0\,4n+1)$ reflection.** Bond centers are numbered in Fig. S2c, and q_1 and q_2 are independent parameters representing static quadrupole moments. The scattering amplitudes F^Q are expressed in terms of $c = 4(1-i)$ and q_1 and q_2. For Γ_4 structure, the azimuth profile is shown for $q_2 = 0$.

4. Microscopic processes for resonant x-ray scattering from the quadrupoles

Here, we discuss possible microscopic processes that lead to resonant x-ray scattering from bond-centered quadrupoles. As discussed in Ref. 15, quadrupole channel has vanishing intensity when only on-site processes are considered.
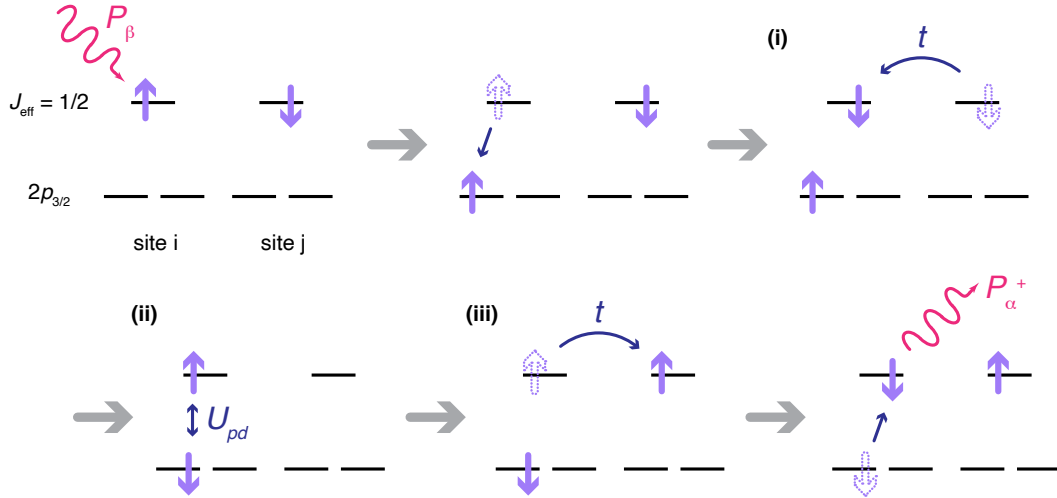
FIG. S4. **Two-site resonant x-ray scattering process**. The bond-centered quadrupoles obtain finite scattering amplitude from inter-site hopping t and on-site Coulomb interaction U_{pd}. The scattering process is illustrated in the hole picture.

The lowest-order RIXS process sensitive to bond-centered quadrupoles is depicted in Fig. S4, which involves (i) hopping to a neighboring site, (ii) exchange scattering between $2p$ core hole and $5d$ valence electron, and (iii) hopping back to the original site, thus having an amplitude smaller than the on-site processes by a factor $\sim t^2 \frac{U_{pd}}{\Gamma^3}$. Specifically, the RIXS

operator $\hat{R}_{\alpha\beta}$ reads:

$$\hat{R}_{\alpha\beta} \propto \sum_{\{m,m'\}} \langle i | \hat{P}_\alpha^+ \frac{\hat{t}}{\Gamma} | m \rangle \langle m | \frac{\hat{U}_{pd}}{\Gamma} | m' \rangle \langle m' | \frac{\hat{t}}{\Gamma} \hat{P}_\beta | i \rangle \, , \qquad (S12)$$

where $\hat{P}_\beta$ ($\hat{P}_\alpha^+$) corresponds to the dipole transition operator for x-rays with polarizations β (α); $|i\rangle$ is the initial state, and $|m\rangle$, $|m'\rangle$ are intermediate states; $\hat{t}$ denotes electron hopping, $\hat{U}_{pd}$ denotes exchange Coulomb interaction between core and valence holes, and Γ is a core-hole lifetime. The energy denominators of this perturbation expansion are replaced by Γ using the fast-collision approximation [16, 17].Alternatively, quadruoples may be detected through inter-site photon-induced transitions (see Fig. S5), as discussed in Refs. 18, 19.
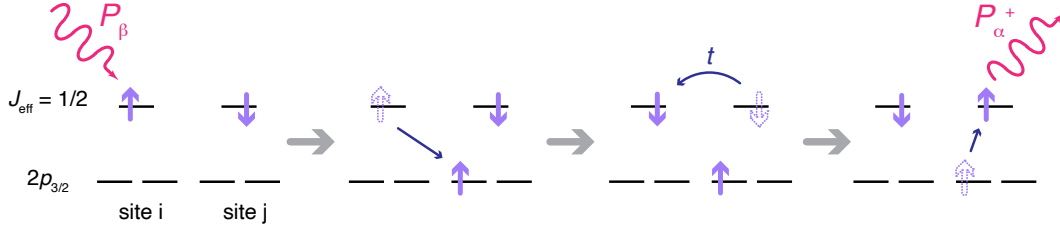
FIG. S5. **Resonant x-ray scattering process with inter-site photon-induced transitions.** The scattering process is illustrated in hole picture.

5. Two-site model calculation

An arbitrary wavefunction $|\Psi\rangle$ for a pair of $S = 1/2$ spins in a 4D Hilbert space can be expressed by eight real numbers u_α and v_α ($\alpha = s, x, y, z$), which are real and imaginary part, respectively, of the coefficients of the usual time-reversal invariant basis for two $S=1/2$ spins; i.e., $|s\rangle = \frac{1}{\sqrt{2}}(|\uparrow\downarrow\rangle - |\downarrow\uparrow\rangle)$, $|x\rangle = \frac{i}{\sqrt{2}}(|\uparrow\uparrow\rangle - |\downarrow\downarrow\rangle)$, $|y\rangle = \frac{1}{\sqrt{2}}(|\uparrow\uparrow\rangle + |\downarrow\downarrow\rangle)$, and

$|z\rangle = \frac{-i}{\sqrt{2}}(|\uparrow\downarrow\rangle + |\downarrow\uparrow\rangle))$. In this basis, the order paramaters are

$$M_\alpha = -i \sum_{\beta,\gamma\in\{x,y,z\}} \epsilon_{\alpha\beta\gamma}|\beta\rangle\langle\gamma| \,,$$

$$N_\alpha = i(|\alpha\rangle\langle s| - |s\rangle\langle\alpha|) \,,$$

$$Q_{\alpha\beta} = -\frac{1}{2}(|\alpha\rangle\langle\beta| + |\beta\rangle\langle\alpha|) + \frac{1}{3}\delta_{\alpha\beta}|\gamma\rangle\langle\gamma| \,,$$

$$\mathbf{S}^i \cdot \mathbf{S}^j = \frac{1}{4} \sum_{\alpha\in\{x,y,z\}} |\alpha\rangle\langle\alpha| - \frac{3}{4}|s\rangle\langle s| \,.$$

(S13)

First, we note that $\mathbf{M} = 2\,\mathbf{u}' \times \mathbf{v}'$, where $\mathbf{u}' \equiv (u_x, u_y, u_z)$ and $\mathbf{v}' \equiv (v_x, v_y, v_z)$, and thus requiring $\mathbf{M} \parallel \hat{y}$ eliminates two parameters as $u_y = v_y = 0$. Next, we redefine $\mathbf{u}'$ and $\mathbf{v}'$ in the 3-dimensional space (x, s, z), and require that $|\mathbf{u}'|^2 + |\mathbf{v}'|^2 = 1$ (normalization of $|\Psi\rangle$) and $\mathbf{u}' \cdot \mathbf{v}' = 0$ (fixing the overall phase). Note that $\mathbf{u}' \times \mathbf{v}' = \frac{1}{2}(N_z, M_y, -N_x)$. Thus, when $\phi_c = 0$, $\mathbf{u}' \times \mathbf{v}' \parallel \hat{z}$, which means that both $\mathbf{u}'$ and $\mathbf{v}'$ are in the xs plane and can be expressed as

$$\mathbf{u}' = \cos\theta(-\sin\phi,\ \cos\phi,\ 0),$$

$$\mathbf{v}' = \sin\theta(\quad\cos\phi,\ \sin\phi,\ 0).$$

(S14)

Finally, spin canting by angle ϕ_c can be achieved by rotating in the sz plane, whereby

$$\mathbf{u}' = \cos\theta(-\sin\phi,\ \cos\phi\cos\phi_c,\ \cos\phi\sin\phi_c),$$

$$\mathbf{v}' = \sin\theta(\quad\cos\phi,\ \sin\phi\cos\phi_c,\ \sin\phi\sin\phi_c).$$

(S15)

As shown in Eq. (5) in the main text, the wavefunction $|\Psi\rangle$ can be expressed in terms of the two parameters θ and ϕ as

$$|\Psi\rangle = (\cos\theta\cos\phi + i\sin\theta\sin\phi)\cos\phi_c|s\rangle$$

$$+ (-\cos\theta\sin\phi + i\sin\theta\cos\phi)|x\rangle$$

$$+ (\cos\theta\cos\phi + i\sin\theta\sin\phi)\sin\phi_c|z\rangle.$$

(S16)

Using this form of the wavefucntion, the expectation values for the magnetic and non-magnetic order parameters are found as

$$\langle N_x \rangle = \sin 2\theta\cos\phi_c,$$

(S17)

$$\langle M_y \rangle = \sin 2\theta\sin\phi_c,$$

(S18)

$$\langle Q_{xy} \rangle = \langle Q_{yz} \rangle = 0,$$

(S19)

$$\langle Q_{zx} \rangle = \frac{1}{2}\cos 2\theta\sin 2\phi\sin\phi_c,$$

(S20)

$$\langle -\vec{S}^1 \cdot \vec{S}^2 - \frac{1}{4} \rangle = \frac{1}{2}\left(\cos 2\theta\cos 2\phi\cos^2\phi_c - \sin^2\phi_c\right).$$
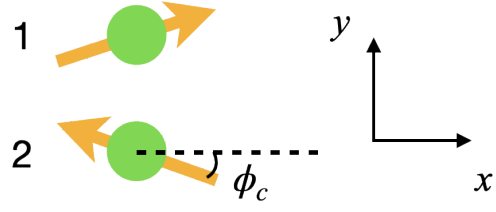
(S21)

FIG. S6. **Two canted magnetic moments.** Two spins are canted by an angle ϕ_c with respect to the global crystal axes x and y, producing a net ferromagnetic moment along the y-axis.

6. Polarization analysis in RIXS

The backscattering-type RIXS spectrometer widely used in the hard x-ray energy regime based on the Rowland circle geometry [20] does not allow polarization analysis because the large angular spread of scattered x-rays precludes the use of a conventional polarizer. However, in our particular case, a judicious selection of the scattering geometry in combination with external magnetic fields allows isolation of all three spin components S_{aa}, S_{bb} and S_{cc}. We note that, for the case of Sr_2IrO_4 with low-spin d^5 configuration, the RIXS operator at Ir L_3-edge can be expressed in terms of spin operators [15].

Fig. S7a shows the magnetic stacking pattern of Sr_2IrO_4 with and without a magnetic field. With a relatively small magnetic field ($\gtrsim$ 0.3 T), magnetic moments can be aligned perpendicular to the field [14]. The $(1\,0\,L)$ scan of Sr_2IrO_4 with a magnetic field in Fig. S7b demonstrates that domains are well aligned by the field in our experiment, showing a completely suppressed $(1\,0\,4n)$, mostly suppressed $(1\,0\,4n+2)$, and dominant $(1\,0\,2n+1)$ peaks [21]. Thus, the orientation of the magnetic moments can be controlled by rotating the magnet holder which changes the direction of the field.

In addition, a large momentum transfer from the high energy of x-rays provides access to multiple Brillouin zones allowing measurements in many different scattering geometries. Specifically, the incident angle α in Fig. S7c can be varied from almost zero to 90°. To align the crystallographic axes to the magnetic field, the sample is oriented so that the ac-plane is in the scattering plane, and the scattering angle (2θ) is fixed close to 90° to suppress elastic Thomson scatterings. Under these conditions, the RIXS responses at extreme incident angles, normal ($\alpha \sim 90°$) or grazing ($\alpha \sim 0°$), are sensitive mostly to two spin components.

For example, in a normal-incidence geometry ($\alpha \sim 90°$), two polarization channels, $\pi \times \pi'$ and $\pi \times \sigma'$, mostly measure S_{bb} and S_{cc}, respectively. When a magnetic field is applied along [010], the weak ferromagnetic moments in Sr_2IrO_4 are fully aligned parallel to the field direction (Fig. S7a) and all spins are aligned to the perpendicular direction [100]. Thus, RIXS in a normal-incidence geometry with a [010] field collects the two transverse modes (T+T') to the AF moments, where T is the in-plane transverse mode and T' is the out-of-plane transverse mode. On the other hand, when the field is applied along [100], the longitudianl (L) and the out-of-plane (T') modes are collected. Likewise, the modes being measured in a grazing-incidence geometry can be determined for each field direction,
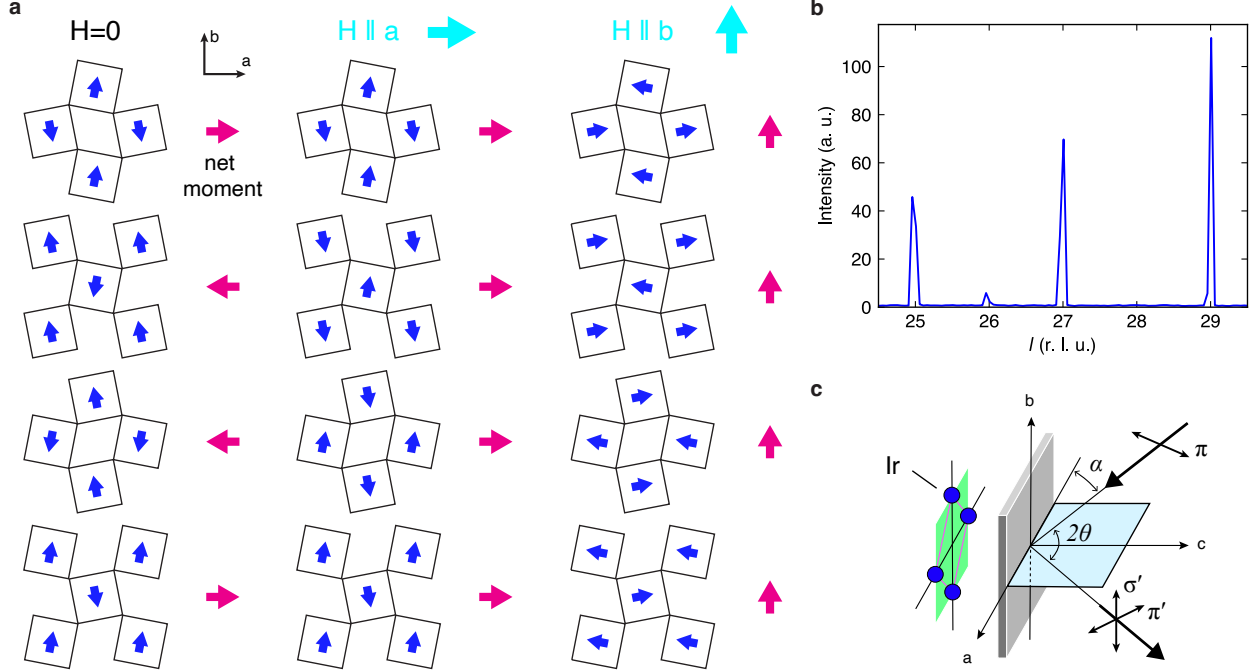
FIG. S7. **Polarization analysis of RIXS measurements**. **a,** Magnetic ordering pattern of Sr_2IrO_4 with and without a magnetic field. Without a magnetic field, canted pseudospin moments (blue arrows) in each IrO_2 planes produce a net ferromagnetic moments (magenta arrows) with a stacking pattern of '*uddu*' along the c-axis. With a small magnetic field (cyan arrows), the net ferromagnetic moments are aligned along the field direction ($\mathbf{H} \parallel a$ or $\mathbf{H} \parallel b$), rendering pseudospin moments approximately perpendicular to the field direction. **b,** $(1\,0\,L)$ scan with a small magnetic field along the b-axis. **c,** Schematics of scattering geometry for RIXS measurements. α is the incident angle and 2θ is the scattering angle between incident and outgoing x-rays. The c-axis normal sample is oriented such that the ac-plane is the scattering plane. In this horizontal scattering geometry, π-polarized x-rays are incident to the sample and outgoing x-rays are unpolarized.

and the corresponding modes for all possible combinations of incidence geometries and field directions are tabulated in Extended Data Table 1. We note that this idea has been used in previous RIXS studies on Sr_2IrO_4 to suppress [21] or emphasize [22] the out-of-plane transverse mode at (π, π).

In our experiment, we choose to measure RIXS in a normal-incidence geometry varying the field direction. We fixed the scattering geometry because changing the scattering geometry significantly varies the x-ray footprint on the sample which makes a direct comparison

18

of intensities between the spectra difficult. Also, since two spectra obtained in a grazing-incidence geometry practically provide the same polarization components (Extended Data Table 1), we decided to conduct RIXS in a normal geometry which can provide two spectra of T+T′ and T′+L. Since the in-plane (T) and out-of-plane (T′) transverse modes at short wavelengths are virtually identical [21, 23, 24], we can approximate T+T′ and T′+L to 2T and T+L, respectively. Then, the pure transverse (T) and longitudinal (L) mode can be isolated by subtraction/addition of the raw spectra.

We choose $\mathbf{q}$ vectors around (3 0 28.5): (3 0 25.8), (3.5 0 25.8) and (3.5 0.5 25.8) are selected for (π, π), $(\pi/2, \pi/2)$ and $(\pi, 0)$, respectively. A large H value is required to make the incident angle close to normal ($\alpha \sim 90°$). For these $\mathbf{q}$ vectors, the incident angle was around 75°, which gives $\sim 6.7\%$ leakage ($\sin^2 15° \approx 0.067$) in our RIXS spectra. Thus, the contributions to each components (S_{aa}, S_{bb}, S_{cc}) from the two polarization channels, $\pi \times \pi'$ and $\pi \times \sigma'$, are calculated as,

$$\begin{pmatrix} S_{T'+L} \\ S_{T+T'} \end{pmatrix} = \begin{pmatrix} m_a & m_b & m_c \\ n_a & n_b & n_c \end{pmatrix} \begin{pmatrix} S_{aa} \\ S_{bb} \\ S_{cc} \end{pmatrix} , \tag{S22}$$

where m_i and n_i ($i = a, b, c$) are the portions of S_{ii} in the T+T′ spectrum ($S_{T+T'}$) and the T′+L spectrum ($S_{T'+L}$), respectively. However, for Sr_2IrO_4, due to canted moments with a canting angle $\phi \sim 11°$ [14], the in-plane spin components are not exactly parallel to the crystal axes. Thus, another transformation is required to take this into account,

$$\begin{pmatrix} S_{aa} \\ S_{bb} \\ S_{cc} \end{pmatrix} = \begin{pmatrix} \cos^2 \phi & \sin^2 \phi & 0 \\ \sin^2 \phi & \cos^2 \phi & 0 \\ 0 & 0 & 1 \end{pmatrix} \begin{pmatrix} S_L \\ S_T \\ S_{T'} \end{pmatrix} , \tag{S23}$$

where moments are aligned along the a-axis. Given that T and T′ are virtually identical away from the zone center, we find the relation between spin polarized spectra ($S_{\parallel}$, $S_{\perp}$) and raw spectra ($S_{T+T'}$, S_{T+L}) using Eq. (S22) and Eq. (S23), where $S_{\parallel}$ is the spectrum for the pure longitudinal mode and $S_{\perp}$ is for the pure transverse mode. For example, in our experiment, the transformation matrix for $(\pi, 0)$ spectra is given by,

$$\begin{pmatrix} S_{\parallel} \\ S_{\perp} \end{pmatrix}_{(\pi,0)} = \begin{pmatrix} 2.198 & -1.198 \\ -0.118 & 1.118 \end{pmatrix} \begin{pmatrix} S_{T'+L} \\ S_{T+T'} \end{pmatrix}_{(\pi,0)} . \tag{S24}$$
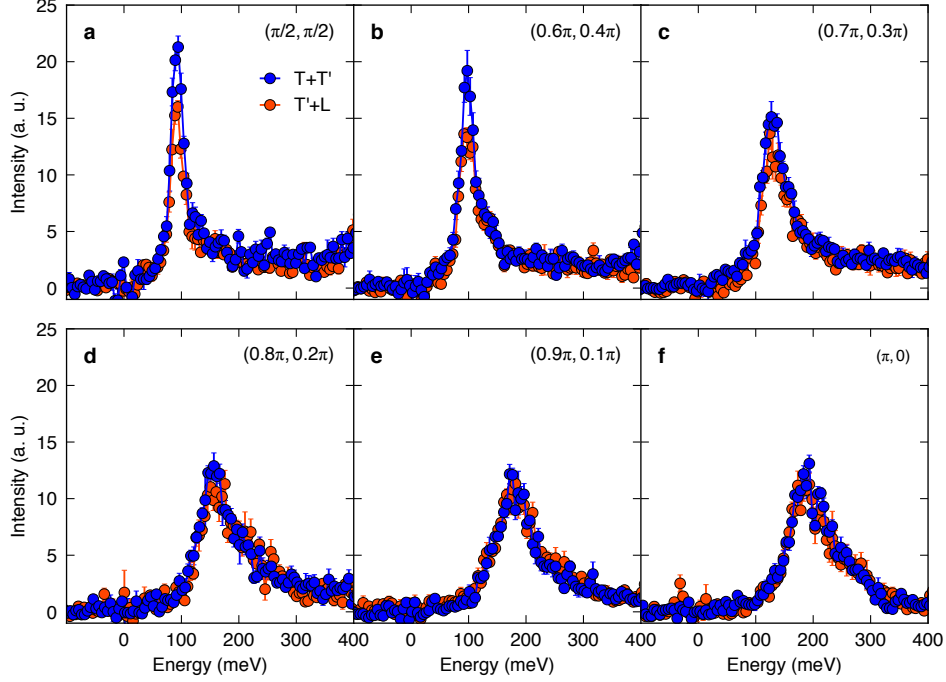
FIG. S8. **Raw RIXS spectra of Sr_2IrO_4. a-f,** The raw RIXS spectra measured along the magnetic zone boundary from $(\pi/2, \pi/2)$ to $(\pi, 0)$. Elastic peaks and constant backgrounds have been removed by fittings. All spectra are normalized to the intensity of electronic excitations $(10Dq)$. The error bars are the standard errors of multiple measurements.

Figure S8 shows the raw RIXS spectra after removing the elastic peaks by fitting. With the vertical (horizontal) magnetic field, the spectrum approximately measures the T+T′ (T+L) components. From the $(\pi/2, \pi/2)$ spectra, it is seen that the peak in the T+T′ channel is much larger than that in the T+L channel due to the single magnon in the T channel. Upon approaching $(\pi\ 0)$, the difference between the two channels gradually decreases, and eventually become identical at $(\pi, 0)$. The error bars in Fig. 4 in the main text were determined by the standard propagation of uncertainty.

We note that a small magnetic field we used here (~ 0.3 T) does not change magnetic excitations in RIXS measurements as demonstrated in Fig. S9, since the magnitude of the in-plane spin exchange (J) in Sr_2IrO_4 is about 60 meV while a field of 0.3 T corresponds to 57 μeV for a 1 μB spin.
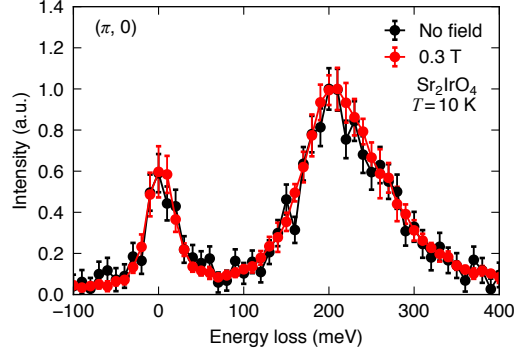
FIG. S9. **Field dependence of RIXS spectrum**. The $(\pi, 0)$ spectrum of Sr_2IrO_4 is measured with (black) and without (red) an external magnetic field of 0.3 T. The two raw spectra show no difference within the error bars.

[1] Y. Joly, S. P. Collins, S. Grenier, H. C. N. Tolentino, and M. De Santis, Phys. Rev. B **86**, 220101 (2012).

[2] Y. Tanaka, T. Takeuchi, S. W. Lovesey, K. S. Knight, A. Chainani, Y. Takata, M. Oura, Y. Senba, H. Ohashi, and S. Shin, Phys. Rev. Lett. **100**, 145502 (2008).

[3] Y. Tanaka, T. Kojima, Y. Takata, A. Chainani, S. W. Lovesey, K. S. Knight, T. Takeuchi, M. Oura, Y. Senba, H. Ohashi, and S. Shin, Phys. Rev. B **81**, 144104 (2010).

[4] Y. Tanaka, S. P. Collins, S. W. Lovesey, M. Matsumami, T. Moriwaki, and S. Shin, J. Phys.: Condens. Matter **22**, 122201 (2010).

[5] T. Usui, Y. Tanaka, H. Nakajima, M. Taguchi, A. Chainani, M. Oura, S. Shin, N. Katayama, H. Sawa, Y. Wakabayashi, and T. Kimura, Nat. Mater. **13**, 611 (2014).

[6] S. L. Zhang, G. van der Laan, and T. Hesjedal, Phys. Rev. B **96**, 094401 (2017).

[7] H. A. Dürr, E. Dudzik, S. S. Dhesi, J. B. Goedkoop, G. van der Laan, M. Belakhovsky, C. Mocuta, A. Marty, and Y. Samson, Science **284**, 2166–2168 (1999).

[8] S. D. Matteo, Journal of Physics D: Applied Physics **45**, 163001 (2012).

[9] F. Ye, S. Chi, B. C. Chakoumakos, J. A. Fernandez-Baca, T. Qi, and G. Cao, Phys. Rev. B **87**, 140406 (2013).

[10] D. H. Templeton and L. K. Templeton, Phys. Rev. B **49**, 14850–14853 (1994).

[11] T. Hahn, *International tables for crystallography. Volume A, Space-group symmetry* (Dor-

drecht; London :Published for the International Union of Crystallography by Kluwer Academic Publishers, 2002).

[12] J. Kim, H. Kim, H.-W. J. Kim, S. Park, J.-K. Kim, J. Kwon, J. Kim, H. W. Seo, J. S. Kim, and B. J. Kim, Phys. Rev. Mater. **6**, 103401 (2022).

[13] T. Choi, Z. Zhang, H. Kim, S. Park, J.-W. Kim, K. J. Lee, Z. Islam, U. Welp, S. H. Chang, and B. J. Kim, Adv. Mater. **34**, 2200639 (2022).

[14] B. J. Kim, H. Ohsumi, T. Komesu, S. Sakai, T. Morita, H. Takagi, and T. Arima, Science **323**, 1329–1332 (2009).

[15] B. J. Kim and G. Khaliullin, Phys. Rev. B **96**, 085108 (2017).

[16] J. Luo, G. T. Trammell, and J. P. Hannon, Phys. Rev. Lett. **71**, 287–290 (1993).

[17] M. van Veenendaal, Phys. Rev. Lett. **96**, 117404 (2006).

[18] W.-H. Ko and P. A. Lee, Phys. Rev. B **84**, 125102 (2011).

[19] Z. Xiong, T. Datta, and D.-X. Yao, npj Quantum Mater. **5**, 78 (2020).

[20] Y. Shvyd'ko, J. Hill, C. Burns, D. Coburn, B. Brajuskovic, D. Casa, K. Goetze, T. Gog, R. Khachatryan, J.-H. Kim, C. Kodituwakku, M. Ramanathan, T. Roberts, A. Said, H. Sinn, D. Shu, S. Stoupin, M. Upton, M. Wieczorek, and H. Yavas, J. Electron Spectrosc. Relat. Phenom. **188**, 140 (2013).

[21] J. Porras, J. Bertinshaw, H. Liu, G. Khaliullin, N. H. Sung, J. W. Kim, S. Francoual, P. Steffens, G. Deng, M. M. Sala, A. Efimenko, A. Said, D. Casa, X. Huang, T. Gog, J. Kim, B. Keimer, and B. J. Kim, Phys. Rev. B **99**, 085125 (2019).

[22] J. Bertinshaw, Y. K. Kim, G. Khaliullin, and B. J. Kim, Annu. Rev. Condens. Matter Phys. **10**, 315–336 (2019).

[23] B. Dalla Piazza, M. Mourigal, N. B. Christensen, G. J. Nilsen, P. Tregenna-Piggott, T. G. Perring, M. Enderle, D. F. McMorrow, D. A. Ivanov, and H. M. Rønnow, Nat. Phys. **11**, 62–68 (2015).

[24] N. Ma, G.-Y. Sun, Y.-Z. You, C. Xu, A. Vishwanath, A. W. Sandvik, and Z. Y. Meng, Phys. Rev. B **98**, 174421 (2018).